The Atmospheric Bridge Communicated the $\delta^{13}C$ Decline during the Last Deglaciation to the Global Upper Ocean

Jun Shao[1], Lowell D. Stott[1], Laurie Menviel[2], Andy Ridgwell[3], Malin Ödalen[4,5], Mayhar Mohtadi[6]

[1]Department of Earth Science, University of Southern California, Los Angeles, CA 90089, USA
[2]Climate Change Research Centre and PANGEA, University of New South Wales, NSW 2052, Sydney
[3]Department of Earth Sciences, University of California, Riverside, CA 92521, USA
[4]Department of Meteorology, Bolin Centre for Climate Research, Stockholm University, 106 91 Stockholm, Sweden
[5]Department of Geosciences, University of Arizona, Tucson, AZ 85721, USA
[6]MARUM-Center for Marine Environmental Sciences, University of Bremen, 28359 Germany

Correspondence to: Jun Shao (junshao@usc.edu)

Abstract. During the early part of the last glacial termination (17.2-15 ka) $\delta^{13}CO_2$ declined sharply by 0.3-0.4‰, coincident with a ~35ppm rise in atmospheric pCO_2. A comparable $\delta^{13}C$ decline has been documented in numerous marine proxy records from surface and thermocline-dwelling planktic foraminifera. The planktic foraminiferal $\delta^{13}C$ decline has previously been attributed to a flux of respired carbon from the deep ocean that was subsequently transported within the upper ocean (i.e. 'bottom up' transport) to sites where the signal is recorded. Benthic $\delta^{13}C$ records from the global upper ocean, including a new record we present here from the tropical Pacific, also document a distinct early deglacial $\delta^{13}C$ decline. However, here we provide modeling evidence that rather than respired carbon from the deep ocean being widely propagated directly to the upper ocean, it instead first upwells to the surface in the Southern Ocean, with a negative $\delta^{13}C$ signal being imparted to the global upper ocean via the atmosphere (i.e. 'top down' transport). The model results also suggest that thermocline waters in upwelling systems like the eastern equatorial Pacific,

and even upper-deep waters, can be affected by this atmospheric bridge during the early deglaciation.

1. Introduction

Atmospheric pCO_2 increased by 80-100ppm from the last glacial maximum (LGM) to the Holocene (Marcott et al., 2014; Monnin et al., 2001). During the initial ~35ppm rise in pCO_2 between 17.2 to 15 ka, ice core records also document a contemporaneous 0.3‰ decline in atmospheric $\delta^{13}C$ (Bauska et al., 2016; Schmitt et al., 2012) (Figure 1a, b, interval highlighted in grey). This millennial-scale trend was punctuated by an interval of more rapid change, with a 12ppm pCO_2 increase (Marcott et al., 2014) and a -0.2‰ decrease in $\delta^{13}CO_2$ (Bauska et al., 2016) occurring in an interval of just ~200 years, between 16.3-16.1 ka (Figure 1a, b, interval highlighted in red). Hypotheses proposed to explain these transient perturbations between 17.2 to 15 ka includes increased Southern Ocean ventilation (e.g. Skinner et al., 2010, Burke et al., 2012), poleward shift/enhanced Southern Hemisphere westerlies (Toggweiler et al., 2006, Anderson et al., 2009, Menviel et al., 2018) and reduced iron fertilization (Martínez-García et al., 2014). However, the chain of events leading to the atmospheric changes recorded in ice cores is not well understood.

Marine proxy records can provide further constraints on the possible mechanisms. For instance, during the early deglaciation, surface and thermocline dwelling foraminifera around the global ocean also recorded a distinct $\delta^{13}C$ drop (e.g. Hertzberg et al., 2016; Lund et al., 2019; Spero and Lea, 2002), an observation replicated by shallow benthic records from the tropical/subtropical Atlantic and Indian Ocean (Lynch-Stieglitz et al., 2019; Romahn et al., 2014). These observations have often been interpreted to reflect a spread of high nutrient, low $\delta^{13}C$ waters originating in the

Southern Ocean that were subsequently transported throughout the upper ocean via a so-called intermediate water teleconnection (Martínez-Botí et al., 2015; Pena et al., 2013; Spero and Lea, 2002). According to this hypothesis, formerly sequestered carbon from deep waters were upwelled in the Southern Ocean (Anderson et al., 2009) in response to a breakdown of deep ocean stratification (Basak et al., 2018). This carbon was then carried by Antarctic Intermediate Water (AAIW) and Southern Ocean Mode Water (SAMW) to low latitudes where it was outgassed to the atmosphere in upwelling regions like the eastern equatorial Pacific (EEP) and recorded in ice cores. We term this scenario 'bottom up' transport, with the upper ocean at lower latitudes acting as a conduit for ^{13}C-depleted carbon to enter the atmosphere. The alternative scenario to explain the early deglacial decline in planktic (and shallow benthic) $\delta^{13}C$ we term 'top down'. This recognizes the importance of air-sea exchange significantly influences seawater $\delta^{13}C$ (e.g. Schmittner et al., 2013), with air-sea $\delta^{13}C$ equilibration in the surface layer, followed by propagation of a $\delta^{13}C$ signal from surface to upper intermediate depths occurring on a multi-decadal to centennial timescale (Heimann and Maier-Reimer 1996; Broecker et al., 1985; Eide et al., 2017). Although these time-scales allow for an atmospheric $\delta^{13}C$ decline to be propagated throughout the upper ocean, until recently (Lynch-Stieglitz et al., 2019), this 'top down' effect has been largely ignored in the interpretation of marine planktic and benthic $\delta^{13}C$ records. The 'top down' scenario has very different implications from 'bottom up'. Firstly, a negative $\delta^{13}C$ need not be associated with enhanced nutrient supply to the upper ocean (on the principal that nutrients are trapped in some deep ocean reservoir along with isotopically depleted carbon). Secondly, a 'top down' scenario does not require a specific initial path of carbon to the atmosphere. Outgassing to the atmosphere could occur anywhere at the ocean surface, with a negative $\delta^{13}C$ signal then propagating globally

through air-sea gas exchange – akin on-going fossil fuel CO_2 emissions and the propagation of its isotopically depleted signal down through the ocean (Eide et al., 2017).

In this paper we take two different steps to help elucidate the more likely of the end-member scenarios. Firstly, we present a new benthic $\delta^{13}C$ record from the western equatorial Pacific (WEP) at 566m that fills an important data gap from intermediate water depths in the Pacific basin. The site is located in the pathway of SAMW and AAIW to the upper tropical Pacific and is also shallow enough be sensitive to $\delta^{13}CO_2$ changes in the 'top down' scenario. Secondly, the early deglacial section of the record is interpreted with insights gained from analyzing a transient deglacial simulation conducted with the Earth system model LOVECLIM (Menviel et al., 2018). In this experiment, sequestered respired carbon from the deep and intermediate waters is ventilated through the Southern Ocean, leading to a sharp decline in $\delta^{13}CO_2$, consistent with ice core records. We explicitly evaluate the two different $\delta^{13}C$ transport scenarios by partitioning the simulated carbon pool and its stable isotope signature into a preformed and a respired component. DIC in a water parcel can be partitioned into surface carbon (preformed carbon, DIC_{pref}) that is transported passively by ocean circulation and accumulated respired carbon (DIC_{soft}) since the water parcel was last in contact with the atmosphere. (We omit carbon released from the dissolution of calcium carbonate ($CaCO_3$) in the water column and at the ocean floor, but we evaluate this component in the Supplement) As the LOVECLIM transient experiment does not explicitly simulate preformed or respired carbon, the respired carbon is instead estimated by apparent oxygen utilization (AOU) – the difference between theoretical oxygen saturation at every grid point in the model and simulated [O_2] (see section 2.3). If the 'top down' transport scenario was the mechanism responsible for the $\delta^{13}C$ decline in marine proxy records from the upper 1000m depth, the preformed signal should dominate, while a regenerated signal would dominate in the 'bottom up'

scenario. The carbon partitioning framework is not new - previous studies have used this framework to study the mechanisms that lead to lower glacial atmospheric CO_2 (Ito and Follows, 2005; Khatiwala et al., 2019) and processes that control $\delta^{13}CO_2$ and marine carbon isotope composition (Menviel et al., 2015; Schmittner et al., 2013). This diagnostic framework has also been applied to study the carbon cycle perturbation in response to a weaker Atlantic Meridional Overturning Circulation (AMOC) (Schmittner and Lund, 2015), albeit in experiments that were performed under constant pre-industrial conditions. New here, however, is the creation in a 2nd Earth System model – cGENIE (Cao et al., 2009) – of a comprehensive diagnostic tracer framework (including for the first time a respired organic matter $\delta^{13}C$ tracer) that is employed to fully evaluate the AOU-based off-line approach (SI).

2 Methods

2.1 Stable Isotope Analyses and Age Model for Piston Core GeoB17402-2

The WEP piston core GeoB17402-2 (8°N, 126°34'E, 556m) was recovered from the expedition SO-228. Planktic foraminiferal samples for ^{14}C age dating were picked from the greater than 250μm size fraction of sediment samples and were typically between 2 and 5mg. All new radiocarbon ages were measured at the University of California Irvine Accelerator laboratory. An age model (Figure S1) was developed for this core with BChron using the Marine20 calibration curve (Heaton et al., 2020) without any further reservoir age correction.

For benthic foraminiferal $\delta^{18}O$ and $\delta^{13}C$ measurements approximately 4-8 *Cibicidoides mundulus* (*C. mundulus*) were picked. These samples were cleaned by first cracking the tests open and then sonicating them in deionized water after which they were dried at low temperature. The isotope

measurements were conducted at the University of Southern California on a GV Instruments Isoprime mass spectrometer equipped with an autocarb device. An in-house calcite standard (ultissima marble) was run in conjunction with foraminiferal samples to monitor analytical precision. The one standard deviation for standards measured during the study was less than 0.1‰ for both $\delta^{18}O$ and $\delta^{13}C$. The stable isotope data are reported in per mil with respect to VPDB.

2.2 LOVECLIM Deglacial Transient Simulation

The LOVECLIM model (Goosse et al., 2010) consists of a free-surface primitive equation ocean model (3° × 3°, 20 vertical levels), a dynamic–thermodynamic sea ice model, an atmospheric model based on quasi-geostrophic equations of motion (T21, three vertical levels), a land surface scheme, a dynamic global vegetation model (Brovkin et al., 1997) and a marine carbon cycle model (Menviel et al., 2015). To study the sensitivity of the carbon cycle to different changes in oceanic circulation, a series of transient simulations of the early part of the last deglaciation (19-15ka) (Menviel et al., 2018) was performed by forcing LOVECLIM with changes in orbital parameters (Berger, 1978) as well as Northern Hemispheric ice-sheet geometry and albedo (Abe-Ouchi et al., 2007), and starting from a LGM simulation that best fit oceanic carbon isotopic (^{13}C and ^{14}C) records (Menviel et al., 2017). The simulation we analyzed for this study is "LH1-SO-SHW" from Menviel et al, (2018). This particular simulation was chosen because 1) recent ice core records also suggest enhanced SO westerly winds during Heinrich stadials (Buitzert et al., 2018); 2) "LH1-SO-SHW" matches some of the important observations (e.g. ice core record of atmospheric pCO_2 and $\delta^{13}CO_2$) better than the other scenarios presented in Menviel et al.,(2018); 3) the stronger SO wind stress in "LH1-SO-SHW" leads to an increased transport of AAIW to lower latitudes, which could have impacted the intermediate depths of the global ocean.

We briefly describe the relevant deglacial forcing here. Firstly, a freshwater flux of 0.07 Sv is added into the North Atlantic between 17.6 ka and 16.2 ka, resulting in an AMOC shut down. Secondly, a salt flux is added into the Southern Ocean between 17.2 ka and 16.0 ka to enhance Antarctic Bottom Water (AABW) formation. Due to its relatively coarse resolution, the model could mis-represent the high southern latitude atmospheric or oceanic response to a weaker NADW. Enhanced AABW could have occurred due to a strengthening of the SH westerlies, changes in buoyancy forcing at the surface of the Southern Ocean, opening of polynyas, or sub-grid processes. Lastly, two stages of enhanced Southern Ocean westerlies are prescribed in the simulation at 17.2 ka and at 16.2 ka; this timing generally corresponds to Southern Ocean warming associated with two phases of NADW weakening during Heinrich Stadial 1 (Hodell et al., 2017). For more detail about this experiment, see Menviel et al., (2018).

2.3 Separating $\delta^{13}C$ Anomalies into the Preformed ($\Delta\delta^{13}C_{pref}$) and Respired ($\Delta\delta^{13}C_{soft}$) Component

The published (Menviel et al., 2018) transient LOVECLIM model experiment we analyze here does not include the numerical tracers required to directly attribute the sources of any given change in $\delta^{13}C$ in the model ocean. We hence make approximations from apparent oxygen utilization (AOU) calculated in the model experiment, and assess the errors inherent in this by means of a set of experiments using a 2nd Earth system model – 'cGENIE' (Cao et al., 2009). This approach is detailed as follows (and in Supplement).

We assume the following carbon isotopic mass balance:

$$\delta^{13}C * DIC = \delta^{13}C_{pref} * DIC_{pref} + \delta^{13}C_{soft} * DIC_{soft} + \delta^{13}C_{carb} * DIC_{carb} \quad (1)$$

where DIC, DIC_{pref}, DIC_{soft}, and DIC_{carb}, are the dissolved total inorganic carbon, the preformed, respired organic matter ('Csoft'), and dissolved (calcium) carbonate carbon pools, respectively. $\delta^{13}C_{pref}$, $\delta^{13}C_{soft}$, and $\delta^{13}C_{carb}$, are the corresponding isotopic signatures (as ‰) that contribute to the $\delta^{13}C$ signature of DIC. It is changes in the $\delta^{13}C$ of DIC that we assume foraminiferal records reflect.

Any given observed $\delta^{13}C$ anomaly in the ocean can then be expressed as:

$$\Delta\delta^{13}C = \Delta(\delta^{13}C_{pref} * DIC_{pref} / DIC) + \Delta(\delta^{13}C_{soft} * DIC_{soft} / DIC) + \Delta(\delta^{13}C_{carb} * DIC_{carb} / DIC) \quad (2)$$

The terms on the RHS represent the contribution of the preformed, respired, and dissolved (carbonate) components to the overall $\delta^{13}C$ change, respectively. Since there is no ^{13}C fractionation during $CaCO_3$ formation in the LOVECLIM model, the last term on the RHS can be assumed to be zero (see Supplement).

We use AOU to estimate respired carbon and its contribution to the $\delta^{13}C$ changes: $\Delta(\delta^{13}C_{soft} * DIC_{soft} / DIC) = \Delta(\delta^{13}C_{soft} * AOU * R_{c:-o2} / DIC)$, where $\delta^{13}C_{soft}$ is estimated by the $\delta^{13}C$ of export POC in the overlying water column, $R_{c:-o2}$ = 117:-170.

This leads to:

$$\Delta\delta^{13}C = \Delta(\delta^{13}C_{pref} * DIC_{pref} / DIC) + \Delta(\delta^{13}C_{soft} * AOU * R_{c:-o2} / DIC) \quad (3)$$

The anomaly, defined as the difference between 15 and 17.2 ka, can be expanded as:

$$\delta^{13}C^{15ka} - \delta^{13}C^{17.2ka} = \delta^{13}C_{pref}{}^{15ka} * DIC_{pref}{}^{15ka} / DIC^{15ka} - \delta^{13}C_{pref}{}^{17.2ka} * DIC_{pref}{}^{17.2ka} / DIC^{17.2ka} + \delta^{13}C_{soft}{}^{15ka} * AOU^{15ka} * R_{c:-o2} / DIC^{15ka} - \delta^{13}C_{soft}{}^{17.2ka} * AOU^{17.2ka} * R_{c:-o2} / DIC^{17.2ka} \quad (4)$$

It is well known that AOU likely overestimates the true oxygen utilization, and thus DIC_{soft}, particularly in water masses formed in high latitudes (Bernardello et al., 2014; Ito et al., 2004; Khatiwala et al., 2019, Cliff et al., 2021). However, to what extent these biases will affect the relative contribution of preformed and respired carbon pool on $\delta^{13}C$ anomaly in a carbon cycle perturbation event has not to our knowledge previously been evaluated. To address this, we conducted a benchmark test with cGENIE, which explicitly simulates the contribution of respired carbon to $\delta^{13}C$ of DIC. Specifically, we performed a similar deglacial transient simulation (see section 2.4) and then applied equation (4) to the cGENIE output; the results are then compared with the values that are explicitly simulated by cGENIE. We also conducted a simplified (modern configuration based) analysis of steady state and transient error terms (Figure S2-S6), which we include in Supplement.

2.4 cGENIE Simulations

The cGENIE model is based on a 3-D frictional geostrophic ocean circulation component, plus dynamic and thermodynamic sea ice components, and is configured here at a resolution of 36x36 horizontal grid and 16 vertical layers. cGENIE lacks a dynamical atmosphere with transport and climate feedback instead provided by a 2-D energy-moisture balance atmosphere (Edwards and Marsh, 2005). The low resolution ocean component and highly simplified atmospheric component make cGENIE much less computationally expensive to run than LOVECLIM. This enables us to include a variety of diagnostic tracers including preformed dissolved inorganic carbon (DIC_{pref}) (Ödalen et al., 2018) and respired (DIC_{soft}) carbon, along with their isotopic components. The simplified nature of the model also facilitates multiple sensitivity experiments run to (deep ocean circulation) steady state. The preformed DIC tracer is created by resetting the DIC_{pref} tracer value

at the ocean surface to the value of DIC at each model time-step, and then allowing ocean circulation to transport the preformed tracers conservatively – i.e. no remineralization or other interior ocean geochemical processes are allowed to modify the preformed tracer value. $\delta^{13}C_{pref}$ is treated similarly. (Technically, isotopes are carried explicitly as concentrations in cGENIE, and delta (δ) values only generated in conjunction with bulk concentrations upon output.) For the organic matter regenerated tracers – respired carbon (and for $\delta^{13}C_{soft}$, the ^{13}C component of respired carbon) is added to the tracer field associated with remineralization of both particulate and dissolved organic matter. The tracer fields are also subject to ocean circulation but the values are reset to zero at the surface. A detailed $\delta^{13}C$ tracer decomposition and attribution error analysis is available in the Supplement.

We configure cGENIE based on the idealized 'glacial' boundary conditions of Rae (2020), with reduced greenhouse gas radiative forcing (i.e. independent of the actual atmospheric pCO_2 calculated by the biogeochemical module) and increased zonal planetary albedo profile in the Northern Hemisphere. The spin-up was run for 10,000 years, with prescribed atmospheric pCO_2 = 278ppm, $\delta^{13}CO_2$ = -6.5‰. We then performed a transient simulation with time varying salt/freshwater flux into the North Atlantic and the Southern Ocean as well as wind stress forcing over the Southern Ocean (Figure S7).

3 Results

The new benthic $\delta^{13}C$ record from the intermediate WEP documents a -0.3 to -0.4‰ decline during the early deglaciation (Figure 1c). We are aware that foraminiferal $\delta^{13}C$ can be complicated by temperature and carbonate ion changes (Bemis et al., 2000, Schmittner et al., 2017), and thus may not solely reflect seawater DIC $\delta^{13}C$ changes. Nonetheless, foraminiferal $\delta^{13}C$ changes (especially

benthic foraminifera) are highly correlated with seawater DIC $\delta^{13}C$ changes (Schmittner et al., 2017). The apparent lag between the onset of decline in benthic $\delta^{13}C$ at site GeoB17402-2 (Figure 1c) and in $\delta^{13}CO_2$ appears to be due to the relatively large age model uncertainty below 154cm in the GeoB17402-2 record (median age ~16.2yr), up to 1-2 kyr (2SD) (Figure S1). Despite this age uncertainty, the new benthic record from the tropical Pacific captures a similar $\delta^{13}C$ decline as recorded from similar depth sites in the tropical/subtropical Atlantic and Indian Ocean (Lynch-Stieglitz et al., 2014, 2019; Romahn et al., 2014).

To investigate whether the early deglacial $\delta^{13}C$ decline observed at these sites in the upper ocean is dominated by the preformed or respired component, we analyzed the LOVECLIM transient simulation (Menviel et al., 2018). In that simulation, freshwater input into the North Atlantic leads to reduced North Atlantic Deep Water (NADW) formation. AMOC is significantly weaker than its glacial condition by ~18 ka (Figure 2a), but this has only a minor effect on the atmospheric CO_2 (Figure 2b) and $\delta^{13}CO_2$ (Figure 2c). On the other hand, enhanced ventilation of Antarctic bottom water (AABW) and Antarctic intermediate water (AAIW) between 17.2 and 15 ka leads to an atmospheric CO_2 increase of ~25 ppm and $\delta^{13}CO_2$ decline of -0.35‰ (Figure 2b, 2c). To the North of 50°S in the Pacific, $\delta^{13}C$ change in the upper 1000m (Figure 3a) is dominated by the preformed signal of ~-0.3‰ (Figure 3c), with minor contribution from respired carbon transport within the ocean interior (Figure 3b). These findings support the 'top down' transport scenario and challenges the 'bottom up' transport scenario as the primary mechanism for the $\delta^{13}C$ decline documented in upper ocean proxy reconstructions. The 'top down' scenario is also compatible with the idea of a nutrient teleconnection between the Southern Ocean and low latitudes (Palter et al., 2010; Pasquier and Holzer, 2016; Sarmiento et al., 2004). Figure 3d illustrates that stronger upwelling brings excess nutrients to the surface of the Southern Ocean. Unused nutrients are then transported to low

latitudes within the upper ocean circulation (e.g. through mode waters and thermocline waters). However, a nutrient teleconnection does not, in itself, reflect enhanced flux of ^{13}C-depleted DIC from the deep ocean to low latitudes in a 'tunnel-like' fashion. The $\delta^{13}C$ signal that is transported in the upper ocean has been strongly affected by air-sea gas exchange at the surface of Southern Ocean and therefore, its evolution is different from the nutrient signal in the LOVECLIM simulation. To be clear, the stronger negative $\Delta\delta^{13}C_{pref}$ compared to $\Delta\delta^{13}C_{soft}$ in the upper ocean does not mean respired carbon is not important in the simulation. In fact, the ultimate ^{13}C-depleted carbon source in LOVECLIM is the simulated respired carbon that accumulated in the deep and intermediate waters during the glacial period as a consequence of the imposed weakened deep-water formation. Our results imply that if deep ocean stratification breaks down as it does in the LOVECLIM simulation, ^{13}C-depleted deep waters upwell and the isotopic signal is transmitted to the atmosphere through strong outgassing in the Southern Ocean (Figure 4). Subsequently, air-sea exchange dominates the $\delta^{13}C$ decline in the global upper ocean.

Our cGENIE benchmark test suggests that when the deep Pacific is ventilated through the Southern Ocean, the AOU-based calculation likely overestimates the magnitude of the positive $\Delta\delta^{13}C_{soft}$ and the magnitude of the negative $\Delta\delta^{13}C_{pref}$ in the Southern Ocean (Figure 5). However, to the north of 30°S in the upper 1000m of the Pacific, the offline approach can provide a reasonably good estimate (Figure 5, also Figure S4, S6). The benchmark test thus gives us confidence that the analysis we performed with LOVECLIM is robust.

4 Discussion:

4.1 Atmospheric $\delta^{13}C$ Bridge

The simulated results presented in this study imply that the wide-spread deglacial $\delta^{13}C$ minimum observed in marine planktic and upper intermediate depth benthic records can be explained, to the first order, by air-sea gas exchange. The atmosphere seems to act as a bridge in transmitting a $\delta^{13}C$ signal from sites (i.e. high latitude Southern Ocean in both the LOVECLIM and cGENIE simulation) where ^{13}C-depleted carbon is released to the atmosphere (i.e. high latitude Southern Ocean in both the LOVECLIM and cGENIE simulation) to the global surface and subsurface ocean. A good example is the simulated transient $\delta^{13}C$ minimum event between 16.2 -15.8 ka in LOVECLIM (Figure 2c), which originates from the Southern Hemisphere and specifically from enhanced ventilation of AAIW (Figure 2a). In the model, if the 'top down' scenario is true, the upper water masses away from the Southern Hemisphere would show similar magnitude of $\delta^{13}C$ changes as $\delta^{13}CO_2$, while water masses in the mid or high latitude Southern Hemisphere may show different $\delta^{13}C$ responses due to dynamical circulation and productivity changes induced by Southern Ocean processes. On the other hand, if the 'bottom up' scenario is true, a large negative $\delta^{13}C$ anomaly should first appear in the South Pacific subtropical gyre (STGSP), then progressively spread to the tropics and finally reach the North Pacific; the negative $\delta^{13}C$ anomaly is also likely to be diluted along its pathway from the South Pacific to the North Pacific. In the LOVECLIM simulation, there is no $\delta^{13}C$ minimum in the upstream STGSP, while the atmosphere-like negative $\delta^{13}C$ anomaly appears in the EEP thermocline, the North Pacific subtropical gyre (STGNP) and North Pacific Intermediate Water (NPIW) simultaneously (Figure 6). In addition, millennial-scale $\delta^{13}C$ evolution in these upper ocean water masses to the north of the equator all exhibit a pattern of change that is similar to the atmosphere (Figure 6). The synchronized $\delta^{13}C$ changes therefore point to the dominant role of atmospheric communication rather than time-progressive oceanic transport of a low $\delta^{13}C$ signal in LOVECLIM.

In the LOVECLIM simulation, both millennial- and centennial-scale $\delta^{13}CO_2$ declines are the result of enhanced deep ocean and/or intermediate ocean ventilation through the Southern Ocean. Using the UVic Earth-System model, Schmittner and Lund (2015) showed that a slow-down of AMOC alone is able to weaken the global biological pump and lead to light carbon accumulation in the upper ocean and the atmosphere, without explicitly prescribing any forcing in the Southern Ocean. Despite the different prescribed forcing, $\Delta\delta^{13}C_{pref}$ also dominates the total $\Delta\delta^{13}C$ in the upper 1000m of the global ocean in the UVic experiment (See Figure 6 in Schmittner and Lund, 2015). Taken together, simulations by all three models suggest that any process that lowers $\delta^{13}CO_2$ would have an influence on the global upper ocean $\delta^{13}C$. In fact, the same phenomenon has been recurring since the preindustrial era due to fossil fuel burning - known as the Suess effect (Eide et al., 2017). This limits the use of planktic and upper intermediate depth benthic $\delta^{13}C$ records for identifying source(s) and locations of light carbon released to the atmosphere during the last deglaciation, consistent with what Lynch-Stieglitz et al., (2019) proposed.

4.2 Revisiting EEP Thermocline $\delta^{13}C$

Waters at eastern equatorial Pacific (EEP) thermocline depths are thought to be connected to the deep ocean through AAIW from the south and NPIW from the north. The EEP is therefore a potential conduit for deep ocean carbon release to the atmosphere. Indeed, we find that the LOVECLIM simulated $\delta^{13}C$ changes in the thermocline of the EEP mainly reflects a preformed signal. The EEP is a dynamical region and observed $\delta^{13}C$ variability in its upper waters likely reflects local processes that are not accounted for by the LOVECLIM simulation. However, we would like to highlight two planktic $\delta^{13}C$ records that show strikingly similar evolution to the model simulation (Figure 7, Figure S8). Site GGC17/JPC30 is close to the coast and the wood-

constrained constant surface reservoir ages over the last 20 ka suggest this site was not influenced by old respired carbon from high latitudes (Zhao and Keigwin, 2018). Site ODP1238 is located in the main upwelling region where strengthened CO_2 outgassing inferred from boron isotope data has been interpreted to reflect respired carbon transported from the Southern Ocean (Martínez-Botí et al., 2015). If the deglacial history of subsurface influence was indeed distinctively different at the two sites, the remarkably similar planktic $\delta^{13}C$ evolution provides strong evidence that thermocline $\delta^{13}C$ in the EEP is dominantly controlled by the 'top down' mechanism rather than the 'bottom up' mechanism as previously suggested (Martínez-Botí et al.,2015; Spero and Lea, 2002), consistent with the LOVECLIM simulation (Figure 7). Collectively, our results show that even in strong upwelling regions, where $\delta^{13}CO_2$ signal from above are likely to be erased by outcropping subsurface waters from below, thermocline $\delta^{13}C$ is still subjected to strong atmosphere influences. This implies that the upper few hundred meters of the water column can be influenced by the atmosphere, consistent with our interpretation of the new benthic $\delta^{13}C$ record presented in this study.

4.3 How Deep Can the Negative $\Delta\delta^{13}C_{pref}$ Signal Reach During the Early Deglaciation?

We have shown that given the dominant control of preformed $\delta^{13}C$ component in the upper ocean, some interpretations of planktic $\delta^{13}C$ records might need to be re-evaluated. Our simulations also reveal that an atmospheric influence can reach deeper than thermocline depths and down to upper intermediate depths. Below 1000m, a $\Delta\delta^{13}C_{pref}$ signal from the atmosphere may still exist, but no longer dominates the total $\Delta\delta^{13}C$ as $\Delta\delta^{13}C_{soft}$ becomes increasingly important at depth.

It has been suggested that deglacial $\delta^{13}C$ variability in the waters above 2000m depth in the Atlantic could be driven by air-sea exchange (Lynch-Stieglitz et al., 2019). However, mid-depth

(1800-2100m) benthic $\delta^{13}C$ records from the Brazil margin (~27°S) document an early $\delta^{13}C$ decline of -0.4‰ between 18.3 and 17 ka, preceding the $\delta^{13}CO_2$ decline between 17 and 15 ka (Lund et al., 2019). Lund et al., (2019) suggest these observations seem at odds with the idea that $\delta^{13}C_{pref}$ contributed to $\delta^{13}C$ variability at their site. The observed benthic $\delta^{13}C$ anomaly at these Brazil margin sites are well simulated by LOVECLIM (Figure 8). Prior to 17.2 ka, $\delta^{13}C$ variability at ~2000m depth at the Brazil Margin in the LOVECLIM simulation is dominantly controlled by excess accumulation of respired carbon (indicated by highly negative $\Delta\delta^{13}C_{soft}$, Figure S9b) due to a weak AMOC, while $\Delta\delta^{13}C_{pref}$ is relatively small (Figure S9c). This is consistent with what previous studies have suggested (Lacerra et al., 2017; Lund et al., 2019; Schmittner and Lund, 2015). Interestingly, LOVECLIM also reveals a strong negative $\Delta\delta^{13}C_{pref}$ signal between 17.2 and 15 ka when $\delta^{13}CO_2$ declines (Figure 9c). However, a positive $\Delta\delta^{13}C_{soft}$ (Figure 9b) signal originating from a loss of respired carbon due to enhanced ventilation at those depths completely compensates for the negative $\Delta\delta^{13}C_{pref}$, which leads to no changes in $\delta^{13}C$ in the simulation (Figure 9a), consistent with the proxy observations. These results suggest that, between 17.2 and 15 ka, a negative preformed $\delta^{13}C$ signal from the atmosphere needs to be considered when interpreting benthic $\delta^{13}C$ records from the upper 2000m of the Atlantic. The complexity associated with interpreting marine $\delta^{13}C$ records further underscores the urgent need to develop robust estimates of respired carbon accumulation/release from water masses.

5 Conclusions:

A transient simulation conducted by the LOVECLIM Earth system model is used as a tool to investigate the pathway of low $\delta^{13}C$ signal transport under a prevailing deglacial scenario that involves Southern Ocean processes. We show that ocean-atmosphere gas exchange likely

dominates the negative $\delta^{13}C$ anomalies documented in planktic and intermediate benthic $\delta^{13}C$ records between 17.2 and 15 ka. Numerical simulations further suggest that enhanced Southern Ocean upwelling can transfer $\delta^{13}C$ signals from respired carbon in the deep ocean directly to the atmosphere. Consequently, $\delta^{13}CO_2$ declines and this leaves its imprint on the global upper ocean through air-sea equilibration. $\Delta\delta^{13}C_{pref}$ dominates the upper 1000m and could account for a 0.3-0.4‰ decline in marine planktic records during the early deglaciation, whereas $\Delta\delta^{13}C_{soft}$ becomes increasingly important at deeper depth. At the same time, the amount of upwelling in the Southern Ocean is a forcing imposed on the model rather than directly constrained. It is therefore possible there were other sites where excess carbon was ventilated to the atmosphere during the deglaciation, which would have also affected $\delta^{13}CO_2$. Our findings imply that planktic and upper intermediate benthic $\delta^{13}C$ records do not provide strong constraints on the site or the mechanisms through which CO_2 was released from the ocean to the atmosphere. Interpretation of early deglacial upper intermediate depth benthic $\delta^{13}C$ records also needs to take into account an atmospheric influence. Whereas in the model simulations the source of the atmospheric signal is a direct response to enhanced Southern Ocean upwelling, our results underscore the need to find a way to fingerprint the actual source(s) of ^{13}C-depleted carbon that caused the $\delta^{13}CO_2$ decline.

References:

Abe-Ouchi, A., Segawa, T., and Saito, F.: Climatic Conditions for modelling the Northern Hemisphere ice sheets throughout the ice age cycle, 16, 2007.

Anderson, R. F., Ali, S., Bradtmiller, L. I., Nielsen, S. H. H., Fleisher, M. Q., Anderson, B. E., and Burckle, L. H.: Wind-Driven Upwelling in the Southern Ocean and the Deglacial Rise in Atmospheric CO_2, 323, 1443–1448, https://doi.org/10.1126/science.1167441, 2009.

Basak, C., Fröllje, H., Lamy, F., Gersonde, R., Benz, V., Anderson, R. F., Molina-Kescher, M., and Pahnke, K.: Breakup of last glacial deep stratification in the South Pacific, 359, 900–904, https://doi.org/10.1126/science.aao2473, 2018.

Bauska, T. K., Baggenstos, D., Brook, E. J., Mix, A. C., Marcott, S. A., Petrenko, V. V., Schaefer, H., Severinghaus, J. P., and Lee, J. E.: Carbon isotopes characterize rapid changes in atmospheric carbon dioxide during the last deglaciation, 113, 3465–3470, https://doi.org/10.1073/pnas.1513868113, 2016.

Bemis, B. E., Spero, H. J., Lea, D. W., and Bijma, J.: Temperature influence on the carbon isotopic composition of Globigerina bulloides and Orbulina universa (planktonic foraminifera), 38, 213–228, https://doi.org/10.1016/S0377-8398(00)00006-2, 2000.

Berger, AndréL.: Long-Term Variations of Daily Insolation and Quaternary Climatic Changes, 35, 2362–2367, https://doi.org/10.1175/1520-0469(1978)035<2362:LTVODI>2.0.CO;2, 1978.

Bereiter, B., Eggleston, S., Schmitt, J., Nehrbass-Ahles, C., Stocker, T. F., Fischer, H., Kipfstuhl, S., and Chappellaz, J.: Revision of the EPICA Dome C CO_2 record from 800 to 600 kyr before present: Analytical bias in the EDC CO_2 record, 42, 542–549, https://doi.org/10.1002/2014GL061957, 2015.

Bernardello, R., Marinov, I., Palter, J. B., Sarmiento, J. L., Galbraith, E. D., and Slater, R. D.: Response of the Ocean Natural Carbon Storage to Projected Twenty-First-Century Climate Change, 27, 2033–2053, https://doi.org/10.1175/JCLI-D-13-00343.1, 2014.

Broecker, W. S., Peng, T.-H., Ostlund, G., and Stuiver, M.: The distribution of bomb radiocarbon in the ocean, J. Geophys. Res., 90, 6953, https://doi.org/10.1029/JC090iC04p06953, 1985.

Brovkin, V., Ganopolski, A., and Svirezhev, Y.: A continuous climate-vegetation classification for use in climate-biosphere studies, 101, 251–261, https://doi.org/10.1016/S0304-3800(97)00049-5, 1997.

Buizert, C., Sigl, M., Severi, M., Markle, B. R., Wettstein, J. J., McConnell, J. R., Pedro, J. B., Sodemann, H., Goto-Azuma, K., Kawamura, K., Fujita, S., Motoyama, H., Hirabayashi, M., Uemura, R., Stenni, B., Parrenin, F., He, F., Fudge, T. J., and Steig, E. J.: Abrupt ice-age shifts in southern westerly winds and Antarctic climate forced from the north, Nature, 563, 681–685, https://doi.org/10.1038/S91586-018-0727-5, 2018.

Burke, A. and Robinson, L. F.: The Southern Ocean's Role in Carbon Exchange During the Last Deglaciation, Science, 335, 557–561, https://doi.org/10.1126/science.1208163, 2012.

Cao, L., Eby, M., Ridgwell, A., Caldeira, K., Archer, D., Ishida, A., Joos, F., Matsumoto, K., Mikolajewicz, U., Mouchet, A., Orr, J. C., Plattner, G.-K., Schlitzer, R., Tokos, K., Totterdell, I., Tschumi, T., Yamanaka, Y., and Yool, A.: The role of ocean transport in the uptake of anthropogenic CO_2, 6, 375–390, https://doi.org/10.5194/bg-6-375-2009, 2009.

Cliff, E., Khatiwala, S., and Schmittner, A.: Glacial deep ocean deoxygenation driven by biologically mediated air–sea disequilibrium, Nat. Geosci., 14, 43–50, https://doi.org/10.1038/S91561-020-00667-z, 2021.

Edwards, N. R. and Marsh, R.: Uncertainties due to transport-parameter sensitivity in an efficient 3-D ocean-climate model, 24, 415–433, https://doi.org/10.1007/s00382-004-0508-8, 2005.

Eide, M., Olsen, A., Ninnemann, U. S., and Eldevik, T.: A global estimate of the full oceanic ^{13}C Suess effect since the preindustrial: Full Oceanic ^{13}C Suess Effect, Global Biogeochem. Cycles, 31, 492–514, https://doi.org/10.1002/2016GB005472, 2017.

Goosse, H., Brovkin, V., Fichefet, T., Haarsma, R., Huybrechts, P., Jongma, J., Mouchet, A., Selten, F., Barriat, P.-Y., Campin, J.-M., Deleersnijder, E., Driesschaert, E., Goelzer, H., Janssens, I., Loutre, M.-F., Morales Maqueda, M. A., Opsteegh, T., Mathieu, P.-P., Munhoven, G., Pettersson, E. J., Renssen, H., Roche, D. M., Schaeffer, M., Tartinville, B., Timmermann, A., and Weber, S. L.: Description of the Earth system model of intermediate complexity LOVECLIM version 1.2, 3, 603–633, https://doi.org/10.5194/gmd-3-603-2010, 2010.

Heaton, T. J., Köhler, P., Butzin, M., Bard, E., Reimer, R. W., Austin, W. E. N., Bronk Ramsey, C., Grootes, P. M., Hughen, K. A., Kromer, B., Reimer, P. J., Adkins, J., Burke, A., Cook, M. S., Olsen, J., and Skinner, L. C.: Marine20—The Marine Radiocarbon Age Calibration Curve (0–55,000 cal BP), Radiocarbon, 62, 779–820, https://doi.org/10.1017/RDC.2020.68, 2020.

Heimann, M. and Maier-Reimer, E.: On the relations between the oceanic uptake of CO_2 and its carbon isotopes, Global Biogeochem. Cycles, 10, 89–110, https://doi.org/10.1029/95GB03191, 1996.

Hertzberg, J. E., Lund, D. C., Schmittner, A., and Skrivanek, A. L.: Evidence for a biological pump driver of atmospheric CO_2 rise during Heinrich Stadial 1: Bio Pump and CO_2 Rise During HS1, 43, 12,242-12,251, https://doi.org/10.1002/2016GL070723, 2016.

Hodell, D. A., Nicholl, J. A., Bontognali, T. R. R., Danino, S., Dorador, J., Dowdeswell, J. A., Einsle, J., Kuhlmann, H., Martrat, B., Mleneck-Vautravers, M. J., Rodríguez-Tovar, F. J., and Röhl, U.: Anatomy of Heinrich Layer 1 and its role in the last deglaciation: HEINRICH EVENT 1, 32, 284–303, https://doi.org/10.1002/2016PA003028, 2017.

Ito, T. and Follows, M. J.: Preformed phosphate, soft tissue pump and atmospheric CO₂, 63, 813–839, https://doi.org/10.1357/0022240054663231, 2005.

Ito, T., Follows, M. J., and Boyle, E. A.: Is AOU a good measure of respiration in the oceans?: AOU AND RESPIRATION, 31, n/a-n/a, https://doi.org/10.1029/2004GL020900, 2004.

Khatiwala, S., Schmittner, A., and Muglia, J.: Air-sea disequilibrium enhances ocean carbon storage during glacial periods, 5, eaaw4981, https://doi.org/10.1126/sciadv.aaw4981, 2019.

Lacerra, M., Lund, D., Yu, J., and Schmittner, A.: Carbon storage in the mid-depth Atlantic during millennial-scale climate events: Mid-depth Atlantic Carbon Storage, 32, 780–795, https://doi.org/10.1002/2016PA003081, 2017.

Lund, D., Hertzberg, J., and Lacerra, M.: Carbon isotope minima in the South Atlantic during the last deglaciation: evaluating the influence of air-sea gas exchange, 14, 055004, https://doi.org/10.1088/1748-9326/ab126f, 2019.

Lynch-Stieglitz, J., Valley, S. G., and Schmidt, M. W.: Temperature-dependent ocean–atmosphere equilibration of carbon isotopes in surface and intermediate waters over the deglaciation, 506, 466–475, https://doi.org/10.1016/j.epsl.2018.11.024, 2019.

Marcott, S. A., Bauska, T. K., Buizert, C., Steig, E. J., Rosen, J. L., Cuffey, K. M., Fudge, T. J., Severinghaus, J. P., Ahn, J., Kalk, M. L., McConnell, J. R., Sowers, T., Taylor, K. C., White, J. W. C., and Brook, E. J.: Centennial-scale changes in the global carbon cycle during the last deglaciation, 514, 616–619, https://doi.org/10.1038/nature13799, 2014.

Martínez-Botí, M. A., Marino, G., Foster, G. L., Ziveri, P., Henehan, M. J., Rae, J. W. B., Mortyn, P. G., and Vance, D.: Boron isotope evidence for oceanic carbon dioxide leakage during the last deglaciation, 518, 219–222, https://doi.org/10.1038/nature14155, 2015.

Martinez-Garcia, A., Sigman, D. M., Ren, H., Anderson, R. F., Straub, M., Hodell, D. A., Jaccard, S. L., Eglinton, T. I., and Haug, G. H.: Iron Fertilization of the Subantarctic Ocean During the Last Ice Age, 343, 1347–1350, https://doi.org/10.1126/science.1246848, 2014.

Menviel, L., Mouchet, A., Meissner, K. J., Joos, F., and England, M. H.: Impact of oceanic circulation changes on atmospheric $\delta^{13}CO_2$: $\delta^{13}CO_2$, 29, 1944–1961, https://doi.org/10.1002/2015GB005207, 2015.

Menviel, L., Yu, J., Joos, F., Mouchet, A., Meissner, K. J., and England, M. H.: Poorly ventilated deep ocean at the Last Glacial Maximum inferred from carbon isotopes: A data-model comparison study: LGM $\delta^{13}C$, 32, 2–17, https://doi.org/10.1002/2016PA003024, 2017.

Menviel, L., Spence, P., Yu, J., Chamberlain, M. A., Matear, R. J., Meissner, K. J., and England, M. H.: Southern Hemisphere westerlies as a driver of the early deglacial atmospheric CO_2 rise, 9, https://doi.org/10.1038/S91467-018-04876-4, 2018.

Monnin, E., Indermuhle, A., Dallenbach, A., Fluckiger, J., Stauffer, B., Stocker, T. F., Raynaud, D., and Barnola, J.-M.: Atmospheric CO_2 Concentrations over the Last Glacial Termination, 291, 112–114, https://doi.org/10.1126/science.291.5501.112, 2001.

Ödalen, M., Nycander, J., Oliver, K. I. C., Brodeau, L., and Ridgwell, A.: The influence of the ocean circulation state on ocean carbon storage and CO₂ drawdown potential in an Earth system model, 15, 1367–1393, https://doi.org/10.5194/bg-15-1367-2018, 2018.

Palter, J. B., Sarmiento, J. L., Gnanadesikan, A., Simeon, J., and Slater, R. D.: Fueling export production: nutrient return pathways from the deep ocean and their dependence on the Meridional Overturning Circulation, 7, 3549–3568, https://doi.org/10.5194/bg-7-3549-2010, 2010.

Pasquier, B. and Holzer, M.: The plumbing of the global biological pump: Efficiency control through leaks, pathways, and time scales: PLUMBING OF THE GLOBAL BIOLOGICAL PUMP, 121, 6367–6388, https://doi.org/10.1002/2016JC011821, 2016.

Pena, L. D., Goldstein, S. L., Hemming, S. R., Jones, K. M., Calvo, E., Pelejero, C., and Cacho, I.: Rapid changes in meridional advection of Southern Ocean intermediate waters to the tropical Pacific during the last 30kyr, 368, 20–32, https://doi.org/10.1016/j.epsl.2013.02.028, 2013.

Rae, J. W. B., Gray, W. R., Wills, R. C. J., Eisenman, I., Fitzhugh, B., Fotheringham, M., Littley, E. F. M., Rafter, P. A., Rees-Owen, R., Ridgwell, A., Taylor, B., and Burke, A.: Overturning circulation, nutrient limitation, and warming in the Glacial North Pacific, 6, eabd1654, https://doi.org/10.1126/sciadv.abd1654, 2020.

Romahn, S., Mackensen, A., Groeneveld, J., and Pätzold, J.: Deglacial intermediate water reorganization: new evidence from the Indian Ocean, 10, 293–303, https://doi.org/10.5194/cp-10-293-2014, 2014.

Sarmiento, J. L., Gruber, N., Brzezinski, M. A., and Dunne, J. P.: High-latitude controls of thermocline nutrients and low latitude biological productivity, 427, 56–60, https://doi.org/10.1038/nature02127, 2004.

Schmitt, J., Schneider, R., Elsig, J., Leuenberger, D., Lourantou, A., Chappellaz, J., Kohler, P., Joos, F., Stocker, T. F., Leuenberger, M., and Fischer, H.: Carbon Isotope Constraints on the Deglacial CO_2 Rise from Ice Cores, 336, 711–714, https://doi.org/10.1126/science.1217161, 2012.

Schmittner, A. and Lund, D. C.: Early deglacial Atlantic overturning decline and its role in atmospheric CO_2 rise inferred from carbon isotopes ($\delta^{13}C$), 11, 135–152, https://doi.org/10.5194/cp-11-135-2015, 2015.

Schmittner, A., Gruber, N., Mix, A. C., Key, R. M., Tagliabue, A., and Westberry, T. K.: carbon isotope ratios (δ13C) in the ocean, 24, 2013.

Schmittner, A., Bostock, H. C., Cartapanis, O., Curry, W. B., Filipsson, H. L., Galbraith, E. D., Gottschalk, J., Herguera, J. C., Hoogakker, B., Jaccard, S. L., Lisiecki, L. E., Lund, D. C., Martínez-Méndez, G., Lynch-Stieglitz, J., Mackensen, A., Michel, E., Mix, A. C., Oppo, D. W., Peterson, C. D., Repschläger, J., Sikes, E. L., Spero, H. J., and Waelbroeck, C.: Calibration of the carbon isotope composition ($\delta^{13}C$) of benthic foraminifera, 32, 512–530, https://doi.org/10.1002/2016PA003072, 2017.

Skinner, L. C., Fallon, S., Waelbroeck, C., Michel, E., and Barker, S.: Ventilation of the Deep Southern Ocean and Deglacial CO2 Rise, Science, 328, 1147–1151, https://doi.org/10.1126/science.1183627, 2010.

Spero, H. J.: The Cause of Carbon Isotope Minimum Events on Glacial Terminations, 296, 522–525, https://doi.org/10.1126/science.1069401, 2002.

Spero, H. J., Mielke, K. M., Kalve, E. M., Lea, D. W., and Pak, D. K.: Multispecies approach to reconstructing eastern equatorial Pacific thermocline hydrography during the past 360 kyr: PAST EASTERN EQUATORIAL PACIFIC HYDROGRAPHY, 18, n/a-n/a, https://doi.org/10.1029/2002PA000814, 2003.

Toggweiler, J. R., Russell, J. L., and Carson, S. R.: Midlatitude westerlies, atmospheric CO_2, and climate change during the ice ages: WESTERLIES AND CO_2 DURING THE ICE AGES, 21, n/a-n/a, https://doi.org/10.1029/2005PA001154, 2006.

Zhao, N. and Keigwin, L. D.: An atmospheric chronology for the glacial-deglacial Eastern Equatorial Pacific, 9, https://doi.org/10.1038/S91467-018-05574-x, 2018.

Data availability. The stable isotope and radiocarbon data are archived on the National Climatic Data Center – NOAA: https://www.ncdc.noaa.gov/paleo-search/study/33094. All modeling data generated or analyzed during this study can be made available upon request to the corresponding author (J.S.).

Author contribution. J.S. designed the research with input from L.S. L.M. provided the LOVECLIM output. A.R. implemented the new diagnostic tracers in cGENIE. J.S. performed the cGENIE simulations with help from A.R. J.S, L.M. and M.Ö analyzed the model simulations. M.M was the chief scientist of the SO-228 expedition and provided samples from the GeoB 17402-2 core. J.S. wrote the manuscript with contributions from all co-authors. A.R. wrote the supplement text.

Competing interests. The authors declare that they have no conflict of interest.

Acknowledgements. This work is supported by the National Science Foundation under Grant Numbers 1558990 (to J.S. and L.S.) and 1736771 (A.R.). L.M. acknowledges funding from the Australian Research Council grant FT180100606. The funding for the expedition SO-228 is from BMBF (German Ministry of Education and Research) grant #03G0228A.

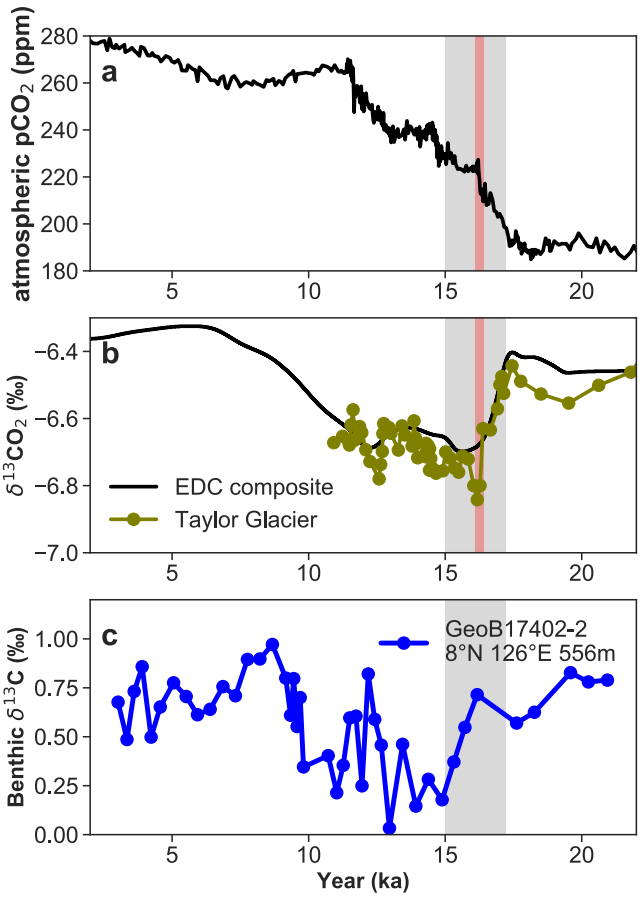

605

Figure 1. a) ice core records of atmospheric CO_2 (Bereiter et al., 2015; Marcott et al., 2014) b) $\delta^{13}CO_2$ records (Bauska et al., 2016; Schmitt et al., 2012) c) *C. mundulus* $\delta^{13}C$ record for upper intermediate depth and mode waters in the western equatorial Pacific. The millennial- and centennial-scale events in these records are highlighted in grey and red, respectively.

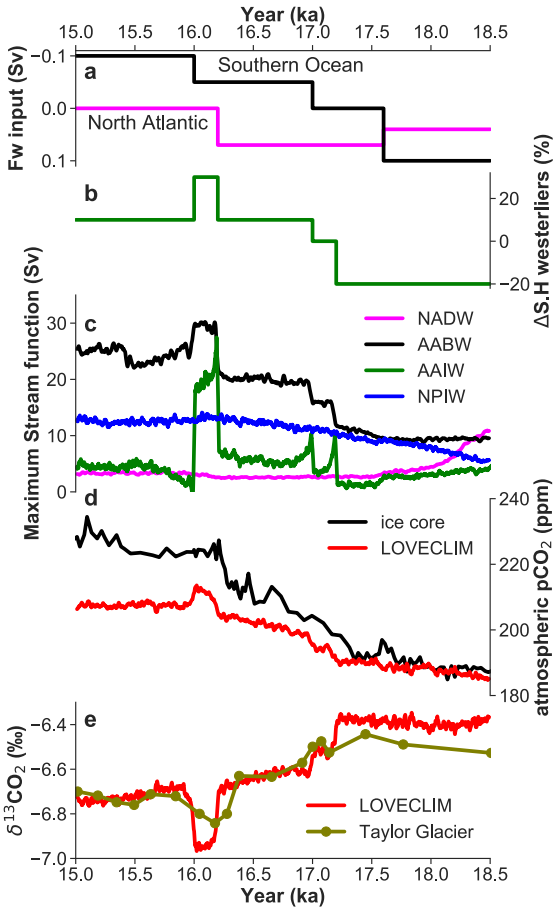

Figure 2. Timeseries from the LOVECLIM transient experiment (Menviel et al., 2018). a) Freshwater input into the North Atlantic and the Southern Ocean; b) Southern Hemisphere westerly wind forcing; c) simulated NADW, AABW, AAIW and NPIW maximum stream function in LOVECLIM. 21-year moving averages are shown for the maximum stream function to filter the high-frequency variability; d) ice core record of atmospheric CO_2 (Bereiter et al., 2015; Marcott et al., 2014) and LOVECLIM simulated atmospheric CO_2; e) The Taylor glacier $\delta^{13}CO_2$ record (Bauska et al., 2016) and LOVECLIM simulated $\delta^{13}CO_2$.

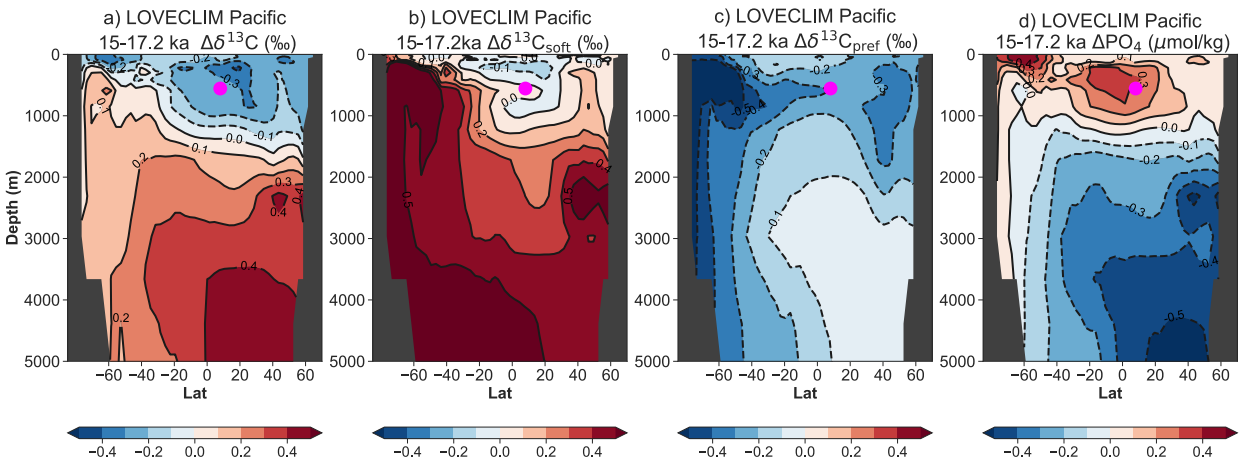

Figure 3. Pacific zonal averaged (160°E-140°W) a) $\delta^{13}C$, b) respired component of $\delta^{13}C$, c) preformed component of $\delta^{13}C$, d) PO_4 anomaly (15ka minus 17.2ka) simulated by LOVECLIM. The magenta circle marks the GeoB17402-2 site.

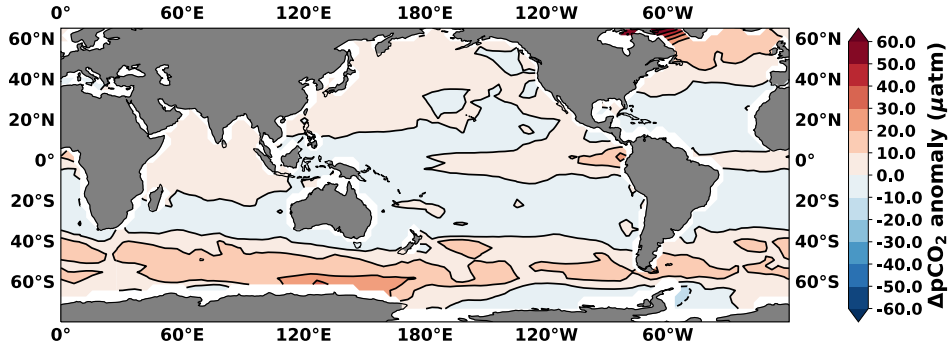

Figure 4. Changes in air-sea surface pCO_2 gradient (15ka minus 17.2ka) simulated by LOVECLIM

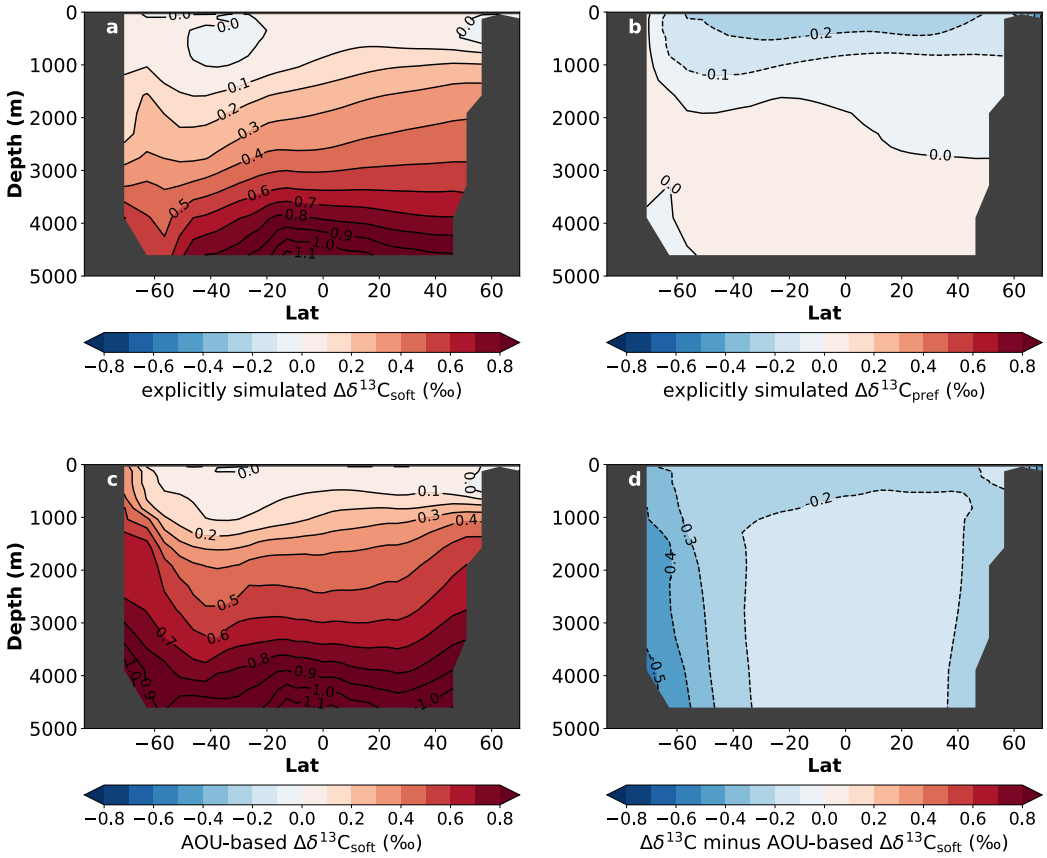

Figure 5. cGENIE benchmark test. The Pacific zonal mean a) respired, b) preformed component of $\delta^{13}C$ anomaly calculated by explicitly simulated tracers (online) and c) respired, d) preformed component of $\delta^{13}C$ anomaly calculated by the AOU-based approach (offline). The anomalies are defined as 15 – 17.2 ka.

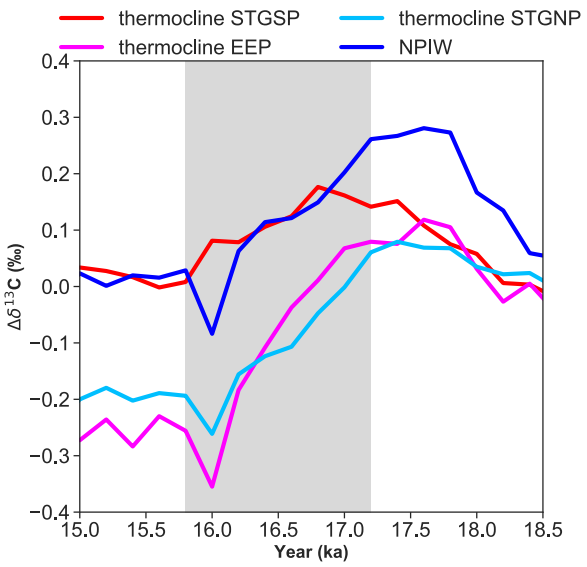

635 **Figure 6. LOVECLIM simulated $\Delta\delta^{13}C$ in thermocline EEP (90-82°W, 5°S-5°N, 77-105m), South Pacific subtropical gyre (STGSP, 160°E- 100°W, 40-22°S, 187-400m), North Pacific subtropical gyre (STGNP, 110°E- 140°W, 22-40°N, 187-400m), NPIW (167-170°E, 54-57°N, 660m. The average of 23.8-20 ka (i.e. LGM) is used as a reference level for the $\Delta\delta^{13}C$ calculations. The interval of decreasing $\delta^{13}C$ is highlighted with a grey bar.**

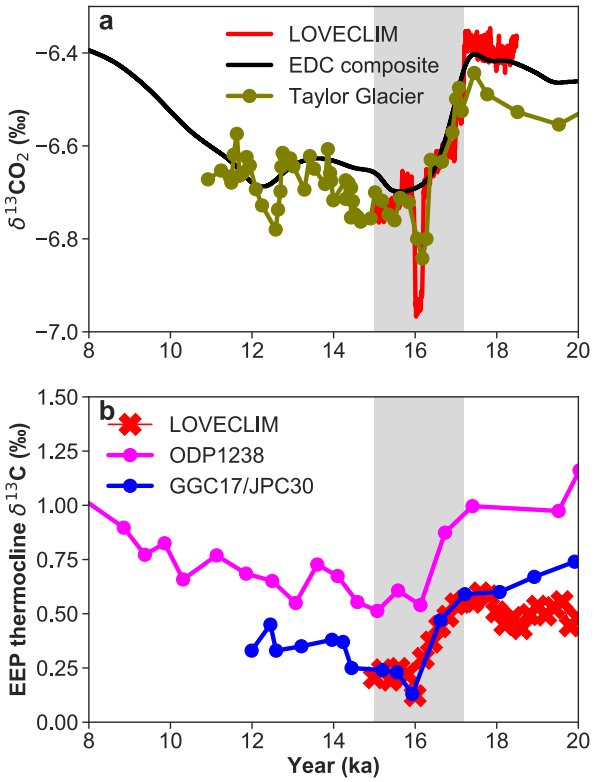

Figure 7. a): $\delta^{13}CO_2$ records (Bauska et al., 2016; Schmitt et al., 2012), simulated $\delta^{13}CO_2$ (21-year running average) in LOVECLIM (Menviel et al., 2018) b): *Neogloboquadrina. dutertrei* (*N. dutertrei*, a shallow thermocline species) $\delta^{13}C$ data from ODP 1238 (Martínez-Botí et al., 2015), GGC17/JPC30 (Zhao and Keigwin, 2018), and LOVECLIM simulated $\delta^{13}C$ of DIC at 100m (average of 82-90°W, 5°S-5°N). The *N. dutertrei* data are corrected by -0.5‰ to normalize to $\delta^{13}C$ of DIC (Spero et al., 2003). The grey shaded bars highlight the time period we focus in this study.

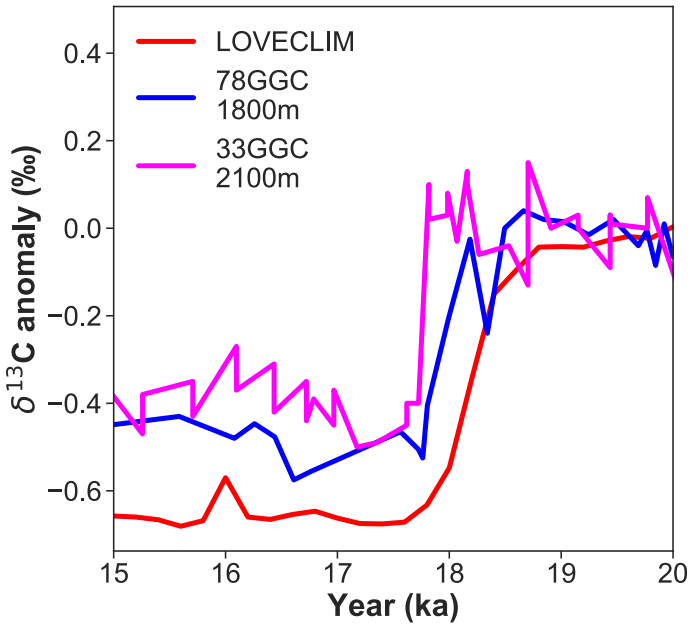

Figure 8. Observed $\delta^{13}C$ anomaly of 78GGC and 33GGC from the mid-depth of Brazil Margin at 27°S (Lund et al., 2015) and simulated $\delta^{13}C$ anomaly at this location.

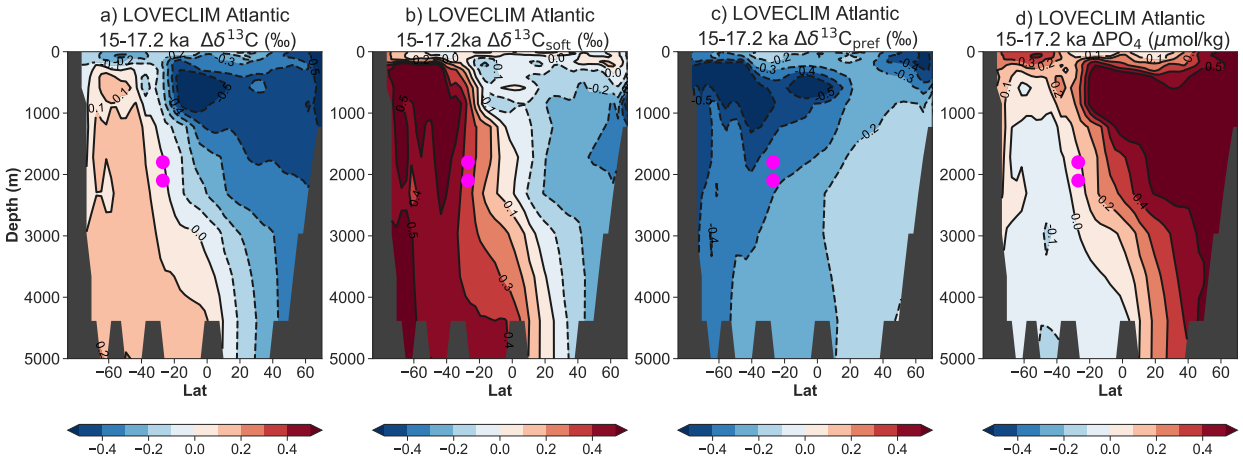

Figure 9. Same as Figure 3, but for the Atlantic zonal averaged (60°W-10°W) anomaly. The location of 78GGC and 33GGC (Lund et al., 2015) are marked as magenta circles.